Spherical Image Processing for Accurate Visual Odometry with Omnidirectional Cameras

Hicham Hadj-Abdelkader, Ezio Malis, Patrick Rives

Spherical Image Processing for Accurate Visual Odometry with Omnidirectional Cameras

Hicham Hadj-Abdelkader, Ezio Malis and Patrick Rives

INRIA Sophia Antipolis - ARobAS team
2004, route des Lucioles - BP93
06902 Sophia Antipolis Cedex - France
{hhadj,emalis,prives}@sophia.inria.fr

Abstract. Due to their omnidirectional view, the use of catadioptric cameras is of great interest for robot localization and visual servoing. For simplicity, most vision-based algorithms use image processing tools (e.g. image smoothing) that were designed for perspective cameras. This can be a good approximation when the camera displacement is small with respect to the distance to the observed environment. Otherwise, perspective image processing tools are unable to accurately handle the signal distortion that is induced by the specific geometry of omnidirectional cameras. In this paper, we propose an appropriate spherical image processing for increasing the accuracy of visual odometry estimation. The omnidirectional images are mapped onto a unit sphere and treated in the spherical spectral domain. The spherical image processing take into account the specific geometry of omnidirectional cameras. For example we can design, a more accurate and more repeatable Harris interest point detector. The interest points can be matched between two images with a large baseline in order to accurately estimate the camera motion. We demonstrate with a real experiment the accuracy of the visual odometry obtained using the spherical image processing and the improvement with respect to the use of a standard perspective image processing.

1 Introduction

Vision-based localization for robotic applications has been widely studied in the literature. In this paper, we consider the general case when a model of the observed scene is not available (see [1–3] techniques supposing that the 3D model of the scene is known). Two complementary approaches to structure from motion estimation have been proposed in the literature: feature-based and template-based approaches. In feature-based approach, geometric features are extracted (e.g. interest points) in each image and then matched (or tracked if the displacement is supposed to be small). Then correct matches (inliers) are obtained using a robust technique and handled to get the camera displacement using for example a RANSAC pose estimation and iterative refinement [4] or a local bundle adjustment technique [5]. This approach can handle large displacements but its accuracy is limited by the precision of features extraction. In template-based

approach, features extraction is avoided since the structure and motion estimation is directly based on image data (the pixel intensities) [6]. This provide a great accuracy in the estimation. However, template based approaches generally fail under very large camera displacements. We exploit the complementarity of these two approaches by using feature-based methods to initialize template-based methods as shown in Fig. 1.

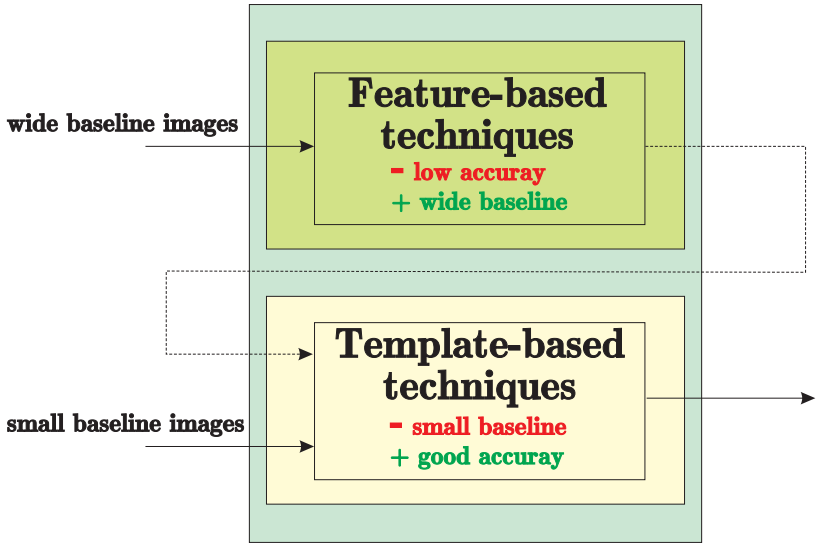

Fig. 1. Efficient approach for accuracy structure and motion

In this paper, we focus on the initialization step. This step should be as fast as possible while providing a reasonable result. Feature-based approaches have showed to provide good performances for perspective cameras. However, there exist only few works that accurately handle the signal distortion that is induced by the specific geometry of omnidirectional cameras. Most of them use the sphere as an appropriate domain for omnidirectional images [7, 8]. Recently, a SIFT approach (feature extraction and matching) for omnidirectional images has been proposed in [9]. The authors showed that processing omnidirectional images on the sphere rather than in the image plane improves the matching performance. Unfortunately, the complete SIFT approach requires multiple scale-space representation which takes too much processing time. On the other hand, a quantitative evaluation of features extraction within the framework of visual SLAM showed that Harris point extractor is much faster than SIFT [10] and more repeatable [11]. Thus, we propose a feature-based approach that combines feature extraction with the Harris interest point detector and features matching with the SIFT descriptors. Our main contribution is to propose a fast and appropriate spherical image processing that take into account the specific geometry of

central omnidirectional cameras. The omnidirectional images are mapped onto a unit sphere and treated in the spherical spectral domain.Thus, we can design a more accurate and more repeatable Harris interest point detector. The interest points can be matched between two images with a large baseline in order to accurately estimate the camera motion. We demonstrate with a real experiment the accuracy of the visual odometry obtained using the spherical image processing and the improvement with respect to the use of a standard perspective image processing.

2 BACKGROUND

2.1 Spherical image for central camera

Omnidirectional imaging systems have taken the interest of researchers in the computer vision community since their wide field of view is suited for many robotic applications such as autonomous navigation or structure from motion. Most of omnidirectional cameras are central and generally based on fish-eye lenses or combine convex mirrors and conventional cameras. It has been shown in [12] that central omnidirectional camera can be modeled using two consecutive projections: spherical projection and perspective one. An intuitive interpretation of this generic model has been proposed in [13] and has been intensively used by the vision and robotics community. Consider $\mathbf{f}$ the generic function of projection of the central camera which maps the 3D point of coordinates $\mathbf{P} = [X \;\; Y \;\; Z]^\top$ to a 2D point of coordinates $\mathbf{p} = [u \;\; v \;\; 1]^\top$ on the image plane:

$$\mathbf{p} = \mathbf{f}(\mathbf{P}, \mathbf{k}) \tag{1}$$

where $\mathbf{k}$ contains the central camera parameters. The inverse function $\mathbf{f^{-1}}$ maps the 2D point on the image plane into the point S on the sphere. The coordinates of S can be expressed using the standard spherical coordinates as:

$$S(\theta, \varphi) = \begin{bmatrix} \sin(\theta)\cos(\varphi) \\ \sin(\theta)\sin(\varphi) \\ \cos(\theta) \end{bmatrix} \tag{2}$$

where $\theta \in [0, \pi]$ and $\varphi \in [0, 2\pi]$ are the colatitude and longitude angles respectively.

If the central camera is calibrated (*ie.* the parameters in $\mathbf{k}$ are known), the omnidirectional image plane $I_p(u, v)$ can be mapped onto the unit sphere to a spherical image $I(\theta, \varphi)$. This mapping can be realized as follow:

– first, the unit sphere is sampled in an equi-angular spherical grid. We use the library s2kit[1] where θ_k and φ_k are given for a bandwidth B by:

[1] is a collection of C routines which compute the discrete Fourier transforms of functions defined on the sphere $\mathbb{S}^2$. Inverse transforms are also provided, as well as convolution routines. This collection can be downloaded from www.cs.dartmouth.edu/∼geelong/sphere/

$$\theta_k = \frac{(2k+1)\pi}{4B} \text{ and } \varphi_k = \frac{\pi k}{B} \tag{3}$$

with $k = 0..2B-1$,

- then, the spherical points S corresponding to the couple (θ, φ) are mapped on the image plane using the projection function $\mathbf{f}$,
- finally, the spherical image is obtained after a local interpolation in the omnidirectional image plane.

An example of the (θ, φ) image and the spherical image of an omnidirectional image given by Fig.2(a) are shown in Fig.2(b) and Fig.2(c) respectively.

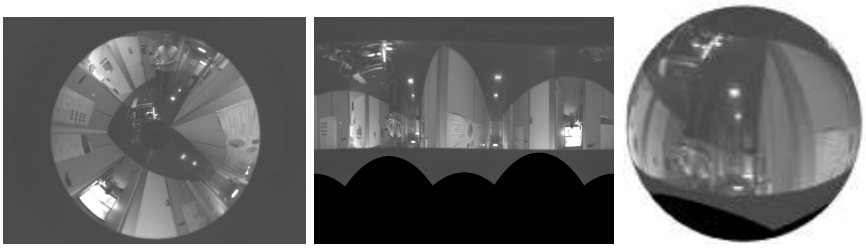

(a) (b) (c)

Fig. 2. Omnidirectional image: (a) original omnidirectional image, (b) (θ, φ) image and (c) spherical image

2.2 Spherical harmonics

In this section, we will recall spherical harmonics tools to deal with square integrable spherical signal $I \in L^2(\mathbb{S}^2)$ which represents the mapped omnidirectional image onto the unit sphere surface.

The spherical signal $I \in L^2(\mathbb{S}^2)$ can be expanded into a linear summation of spherical harmonic functions $Y_{lm} : \mathbb{S}^2 \longrightarrow \mathbb{C}$ of degree l and order m, given by:

$$I = \sum_{l \in \mathbb{N}} \sum_{|m| \leq l} \widehat{I}_{lm} Y_{lm} \tag{4}$$

where $\widehat{I}_{lm}$ are the coefficients of the spherical Fourier transform of the signal I expressed by:

$$\widehat{I}_{lm} = \int_{\mathbb{S}^2} I(\eta) Y^{\star}_{lm}(\eta) d\eta \tag{5}$$

where the symbol $.^{\star}$ denotes the complex conjugate.

The spherical harmonic functions Y_{lm} are given by:

$$Y_{lm} = \sqrt{\frac{2l+1}{4\pi}\frac{(l-m)!}{(l+m)!}}\ P_l^m(\cos(\theta))e^{im\varphi} \tag{6}$$

with $l \in \mathbb{N}$, $\mid m \mid \leq l$ and P_l^m are the associated Legendre polynomials [14].

These spherical harmonic functions can be rotated using the Euler angle decomposition. Let $g \in SO(3)$ expressed in terms of rotations R_z and R_y about the z and $y-$axis respectively. g can thus be written as:

$$g = R_z(\alpha)R_y(\beta)R_z(\gamma) \tag{7}$$

At each element g, a linear operator $\Lambda(g)$ can be associated which acts on a function in $L^2(\mathbb{S}^2)$. The rotated spherical harmonic function is given by:

$$\begin{aligned} \Lambda(g)Y_{lm}(S) &= Y_{lm}(g^{-1}S) \\ &= \textstyle\sum_{|k|\leq l} e^{ik\alpha}\, d^l_{km}(\beta)\, e^{-im\gamma}\, Y_{lk}(S) \end{aligned} \tag{8}$$

where $d^l_{km}(\beta)$ is the Wigner $d-$function. Its explicit expression can be found in [15].

For any spherical function I, a spherical filter h can be applied by correlation. In the case of the planar images, the integration is carried out over the same domain $\mathbb{R}^2$ of the signal and the filter. However, this is no longer true in case of spherical images. Indeed, the convolution has been defined by Wandelt et al in [16] by integrating over $\mathbb{S}^2$ as given in equation (9) and thus the convolution is defined on $SO(3)$.

$$(I \star h)(g) = \int_{\mathbb{S}^2} I(S)h(g^{-1}S)dS \tag{9}$$

In another way, Driscoll and Healy prove in [17] a spherical convolution theorem by integrating over $SO(3)$ and so the result is defined on $\mathbb{S}^2$:

$$(I \star h)(S) = \int_{SO(3)} I(gN)h(g^{-1}S)dg \tag{10}$$

where N is the north pole vector.

If one wants to preserve the convolution result in the same domain as the input functions, the convolution definition given by Driscoll and Healy can be used, and the spectrum of the convolution is:

$$\widehat{(I \star h)}_{lm} = 2\pi\sqrt{\frac{4\pi}{2l+1}}\widehat{I}_{lm}\widehat{h}_{l0} \tag{11}$$

3 SPHERICAL IMAGE PROCESSING IN THE SPECTRAL DOMAIN

In this section, we present details about the spherical image processing using spherical harmonic decomposition. It is well known that image smoothing based

on convolution with gaussian filter is central for image processing and features extraction. However, the gaussian filter designed for perspective images is not adapted for spherical images. In fact, a shift-invariant filter in the planar domain is variant when mapped on the spherical domain. In [18], the spherical gaussian filter has been derived as solution of the heat diffusion equation on the sphere. Its spectrum is given by:

$$\widehat{G}_{lm} = \begin{cases} \sqrt{\frac{2l+1}{4\pi}} e^{-l(l+1)\sigma} & \text{if } m = 0 \\ 0 & \text{else} \end{cases} \tag{12}$$

where σ is the scale factor. Note that the spherical gaussian G is rotational symmetric with respect to the north pole where it is defined. The first draw in Fig. 4 shows an example of the spherical gaussian G.

Feature extraction methods such as corners or edges detection are based on the image derivatives. This can be achieved by convolution with the gaussian derivatives filter [19]. Since the images are defined on the sphere, the spherical gaussian derivatives with respect to the angular coordinates θ and φ must be used:

$$\begin{aligned} \frac{\partial I(\theta,\varphi)}{\partial \theta} &\approx \frac{\partial G}{\partial \theta} \star I(\theta,\varphi) \\ \frac{\partial I(\theta,\varphi)}{\partial \varphi} &\approx \frac{\partial G}{\partial \varphi} \star I(\theta,\varphi) \end{aligned} \tag{13}$$

These derivatives are not trivial to calculate. Indeed, the spherical gaussian is invariant to the azimuthal angle φ since it is defined at the north pole on the sphere, thus $\frac{\partial G}{\partial \varphi} = 0$. Bullow proposed in [8] a solution to compute the derivative along φ in three steps as depicted in Fig. 4. First, the spherical gaussian is shifted from the north pole to the the equator of the sphere by rotation of $\pi/2$ about the $y-$axis using equation (8). Then, the derivative of the spherical gaussian with respect to φ is calculated. Finally, the spherical gaussian derivative is back rotated to the north pole of the sphere. The derivative of the spherical image with respect to φ can be obtained by convolution with the derivative filter. The directional spherical gaussian derivative is not rotationally symmetric filter and however its direction changed when integrating over $SO(3)$ since it is first rotated about the $z-$axis before shifting on the sphere by the two remaining rotations. Thus, the spherical image derivative is not handled correctly.

The spherical gaussian derivative with respect to θ is not considered by Bullow. To our knowledge, the general case has not been yet considered. In the sequel, we show how we can derive the spherical image in the both directions θ and φ using the spectrum of the spherical gaussian derivative filter with respect to φ.

In this work, the spherical image derivatives with respect to θ and φ are correctly achieved. First, we compute the directional spherical gaussian derivative with respect to φ as proposed in [8]. Then, the derivative filter of the spherical gaussian with respect to the colatitude angle θ is obtained by rotating the

derivative filter with respect to longitude angle φ by $\frac{\pi}{2}$ about the $z-$axis in the spectral domain using equation (8). The two derivative filters are shown by the two first draws in Fig. 5. The convolution is achieved by neglecting the first rotation about the $z-$axis as schematized by the two last draws in Fig. 5. This can be realized by integrating over $\mathbb{S}^2$ using the definition (9) and the output is restricted for two angles corresponding to the colatitude and longitudes angles. To compute this convolution, one can use the C routines of the SOFT[2] package. However, these C routines are not adapted. We have rewritten a new mixed Matlab/C routines to compute the convolution with directional spherical gaussian derivatives efficiently. Our algorithms take into account only the two interesting Euler angles α and β. A comparison between the SOFT routines and our routines with respect to the calculation time and the allocation memory is shown in Table 3.

Routines	Bandwidth	Calculation time	Allocation memory
original routines	128	10.2 s	900 KB
	256	out-of-memory	2.5 GB
	512	out-of-memory	19.2 GB
adapted routines	128	0.3 s	1 KB
	256	2 s	9 MB
	512	17 s	35 MB

Fig. 3. Comparison between the original and modified routines used for convolution. Routines are run on a personal computer Pentium D 2.4 GHz - 2 GB DDRAM.

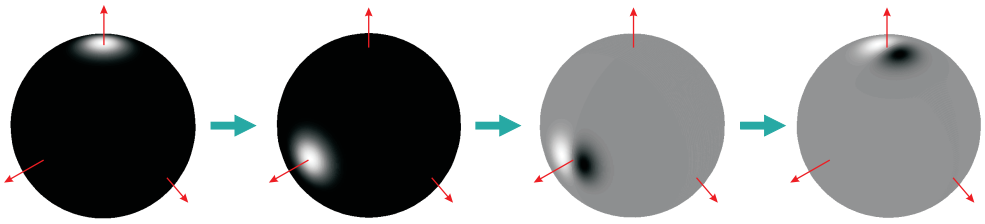

Fig. 4. Spherical gaussian derivative steps with respect to φ

Example of directional spherical gaussian derivatives applied to an omnidirectional image are shown in Fig. 6(a) and Fig. 6(b).

[2] is a collection of C routines which compute the discrete Fourier transform of a function defined on $SO(3)$. This collection can be downloaded from www.cs.dartmouth.edu/∼geelong/sphere/

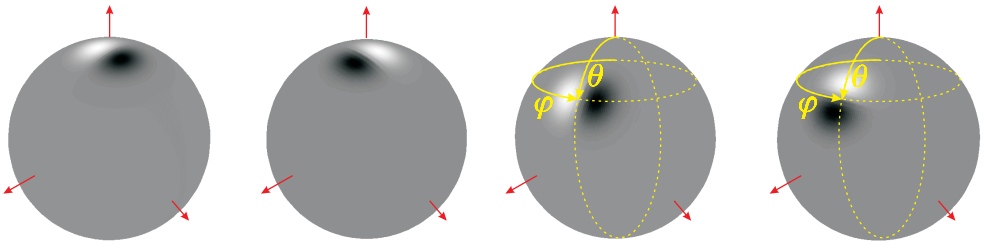

Fig. 5. Convolution with spherical gaussian derivative

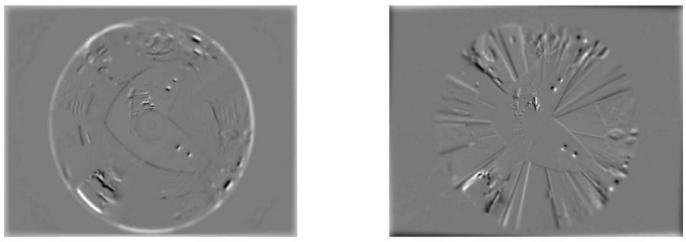

(a) (b)

Fig. 6. directional image derivatives: (a) θ directional derivative, (b) φ directional derivative

4 ACCURATE FEATURE-BASED APPROACH FOR OMNIDIRECTIONAL VISUAL ODOMETRY

We recall that the aim of this work is to design a sufficiently accurate feature-based estimation technique able to initialize the local approaches such as template-based in presence of the wide baseline between successive images.

It is well know that the accuracy of the feature-based approach is depending to the detection precision of the features and their repeatability. In this section, we propose an adapted version of the Harris point detector for omnidirectional images. The algorithm is based on spherical image processing proposed previously. We show with a real experiment the improvement of the precision comparing to the standard approach for perspective images.

4.1 Harris interest point detector for spherical images

Harris detector extracts interest points in an image by evaluating the cornerness of a point. Indeed, points that have high degree of cornerness are selected. The Harris interest point detector is based on the second moment matrix (or autocorrelation matrix) defined by:

$$\mu(\mathbf{x}, \sigma_I, \sigma_D) = \sigma_D^2 G(\sigma_I) \star \begin{pmatrix} I_\theta^2 & I_\theta I_\varphi \\ I_\theta I_\varphi & I_\varphi^2 \end{pmatrix} \tag{14}$$

where $\mathbf{x} = [\theta\ \varphi]^\top$ are the angular coordinates, I_θ and I_φ are the smoothed spherical image derivatives obtained using the proposed technique in this paper, and σ_D and σ_I are the derivative and integration scales respectively.

In order to show the improvement of the adapted Harris detector comparing to the classic Harris detector, we evaluate the repeatability rate r as given in [20]:

$$r(\delta) = \frac{R(\delta)}{\min(N_1, N_2)} \tag{15}$$

where N_1 and N_2 are the number of detected points in the two images and $R(\delta)$ is the number of the corresponding point couples within the neighborhood of size δ after warping all detected points on the same image. Since the warping function is necessary to compute $R(\delta)$, a set of n synthetic images I_k, with $k = 1..n$ are generated by rotating the reference spherical image I_0.

Figures 7(a) and 7(b) show the repeatability rates of the adapted and classical methods. The neighborhood size is fixed to 2 pixels. In figure 7(a), the reference spherical image is rotated by $\alpha_k = k\frac{\pi}{10}$ with $k = 1..20$ about the $z-$axis. In figure 7(b), the reference spherical image is rotated by $\alpha_k = \frac{\pi}{2} - k\frac{\pi}{10}$ with $k = 1..10$ about the $y-$axis. As shown in these two figures, the repeatability rate of points detected with the proposed adapted Harris using spherical images processing is much better then the repeatability obtained by the classical Harris based on the perspective image processing.

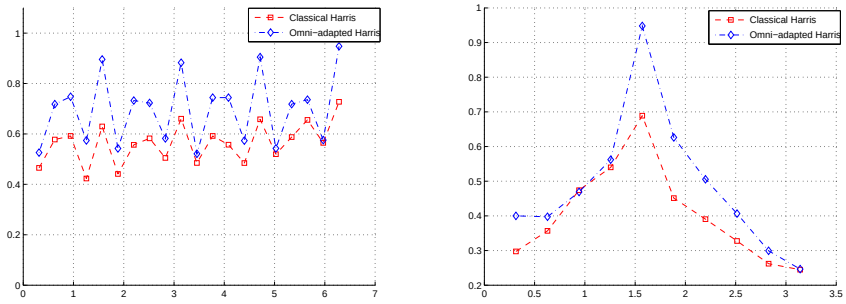

(a) (b)

Fig. 7. Repeatability rate: (a) rotation about $z-$axis , (b) rotation about $y-$axis. On the abscissa, the angles are given in radian

The second step of the feature-based approach is the matching process. Extracted interest points can be matched using for example the SIFT descriptors [21]. The SIFT descriptors are based on the gradient distribution in the detected regions which provide the good results comparing to the other techniques and the robustness to small geometric distortions [11]. However, local regions in omnidirectional images can be significantly distorted under large displacement. Once

more, local image description can be improved for omnidirectional images in the spherical space. In [9], a circular region on the spherical image has been used to build the SIFT descriptors. In this work, the Harris interest points extracted from the spherical image are matched with the adapted SIFT descriptors for spherical image [9].

4.2 Experimental results for the visual odometry

The aim of this experimental evaluation is to illustrate the accuracy of our feature-based technique proposed for omnidirectional camera. The natural way to evaluate our method is to compare it with the existing methods proposed for omnidirectional images. To the best of our knowledge, the first and sole technique was proposed in [9]. Unfortunately, any details about accuracy and time processing have not been provided. We are therefore limited to compare our method to the classic feature-based method where omnidirectional images are handled as perspective images.

The comparison is realized with a sequence of the moving mobile robot in a corridor[3]. The sequence is composed of 600 images with a 1027×768 resolution, acquired by a central catadioptric camera[4] mounted on the mobile robot. The catadioptric camera was calibrated using the open-source matlab toolbox[5] [22]. We suppose that the wheeled odometry of the mobile robot is precise enough and we consider it as the ground truth.

The interest points detection and matching is applied to each pair of images in the sequence with a baseline separation of 20 images. Note that the baseline can be chosen to be more than 20 images but beyond this this value the classical method often failed.

After matching between detected interest points using the two compared methods, the essential matrix $\mathbf{E}$, containing the motion information between the two separated images, is estimated using for example the calibrated fivepoint algorithm proposed in [23] within a RANSAC framework to remove the outliers. Inlier points are used to estimate $\widehat{\mathbf{E}}$ in order to extract the direction of the translation $\widehat{\mathbf{t}}$ and the rotation matrix $\widehat{\mathbf{R}}$.

The visual odometry of the mobile robot can be obtained by integrating the estimated motion between matched images. In this paper, the unknown scale factor is not recovered and we consider only the direction of the translation.

In total, 30 couples of images are matched and used to estimate the motion of the mobile robot. Only some of these couples matching are shown in Fig.8 when using the adapted method for omnidirectional image and in Fig.9 when the classical method is used. As can be shown in these two figures, many false matches are present when using the classical method. This can show clearly that the adapted image processing for omnidirectional image can improve the

[3] the image sequences are provided by C. Mei from University of Oxford

[4] comprised of a S80 parabolic mirror from RemoteReality with a telecentric lens and a perspective camera.

[5] available on http://www.robots.ox.ac.uk/∼cmei/Toolbox.html

precision and the quality of the features detection and matching in presence of the important image deformation due to the large displacement.

In Fig.10, the estimated parameters are shown in dotted lines and the odometry provided by the mobile robot are shown in full lines. Fig.10(a) shows the rotation estimation and Fig.10(c) shows the estimated direction of the translation of the mobile robot by using the proposed adapted method for omnidirectional images. The results of the motion estimation using the classical method are shown by Fig.10(b) for rotation and Fig.10(d) for the direction of the translation.

The rotation error which is the distance between the real rotation $\mathbf{R}$ and the estimated rotation $\widehat{\mathbf{R}}$ using the adapted method (respectively classical method) is shown in Fig.11(a) in full line (respectively dotted line). Fig.11(b) shows the error on the direction of the translation which represent the angle between the two directions of the real translation and the estimated one. In this figure, full line correspond to the error of using the adapted method and the dotted line for using the classical method. As one can see, the motion estimation is improved when taking into account the geometry of the camera. The errors of the estimation using the classical approach are very important comparing to those obtained using our approach. These results confirm that the sphere is an appropriate space to handle omnidirectional images. As shown in Fig.11(a), an important drift appears on classical method comparing to the our method. Note that the deviation does not appear in Fig.11(b) since only the direction of the translation is evaluated and not the intergration of the position.

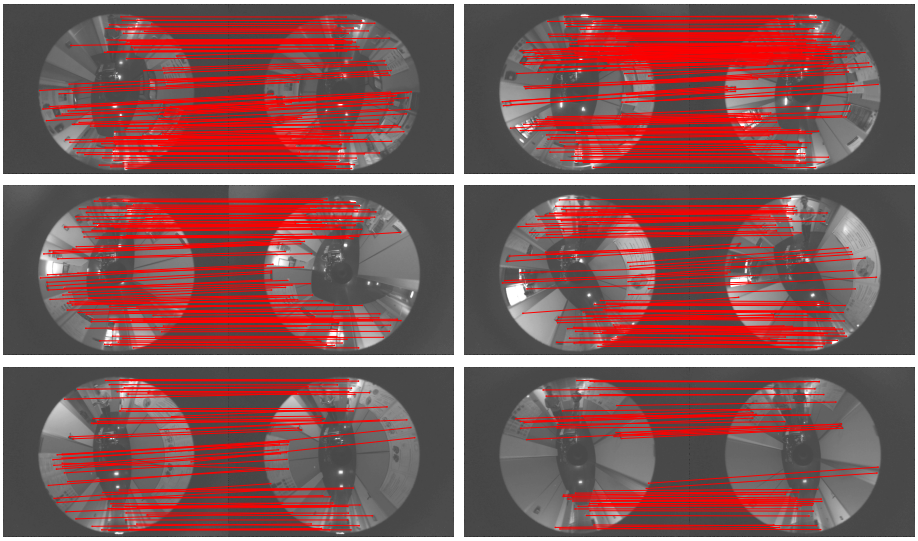

Fig. 8. Features matching using our method between image couples (1,20), (100,120), (220,240), (340,360), (460,480) and (580,600)

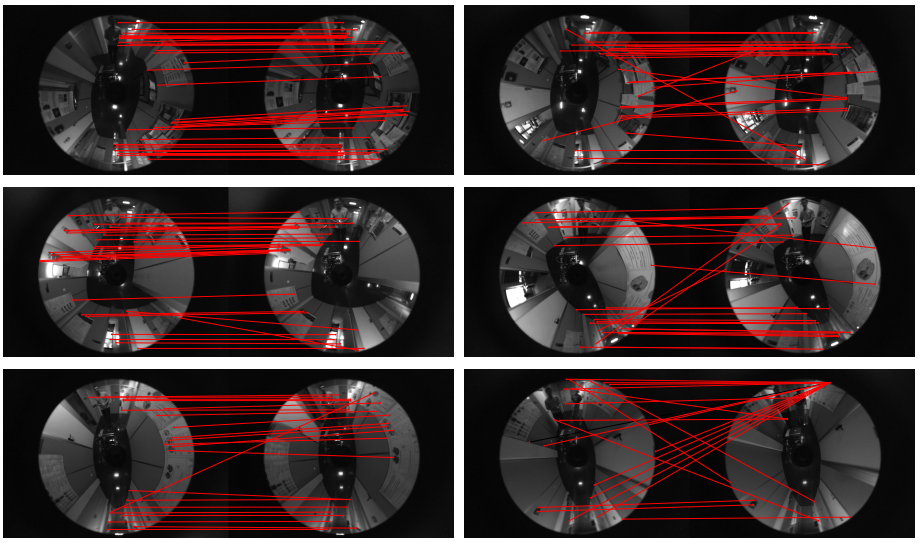

Fig. 9. Features matching using the classical method between image couples (1,20), (100,120), (220,240), (340,360), (460,480) and (580,600)

5 CONCLUSIONS

In this paper, we have proposed an approach for omnidirectional image processing using spherical domain in order to design a feature-based technique able to handle the motion estimation under wide baseline. Spherical image derivatives were presented and used to adapt the Harris interest points detector. We have shown that the proposed Harris detector improves the repeatability and accuracy of the detected interest points. These interest points were matched with an adapted SIFT descriptors to spherical images. The improvement of the proposed approach was validated with real image sequence corresponding to the moving of the mobile robot in the corridor. We have shown through the experimental results that handling omnidirectional images in the spherical space improves the quality of the motion estimates comparing to the existing classical method proposed for perspective images. In the continuation of this work, the accuracy of motion estimates will be improved by initializing the local template-based approach by the proposed feature-based approach in presence of large baseline.

References

1. Drummond, T., Cipolla, R.: Real-time visual tracking of complex structures. IEEE Trans. Pattern Anal. Mach. Intell. **24**(7) (2002) 932–946
2. Comport, A.I., Marchand, E., Chaumette, F.: Real-time markerless tracking for augmented reality: The virtual visual servoing framework. IEEE Transactions on Visualization and Computer Graphics **12**(4) (2006) 615–628

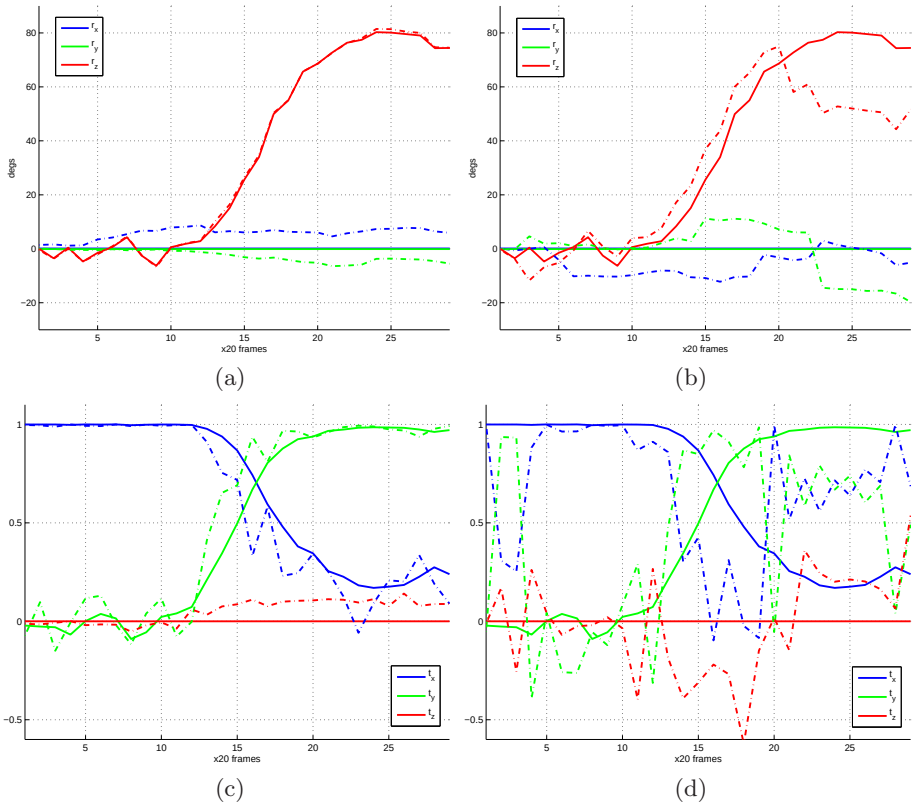

Fig. 10. Motion estimation: (a) rotation and (c) direction of the translation estimated with our method, (b) rotation and (d) direction of the translation estimated with the classical method

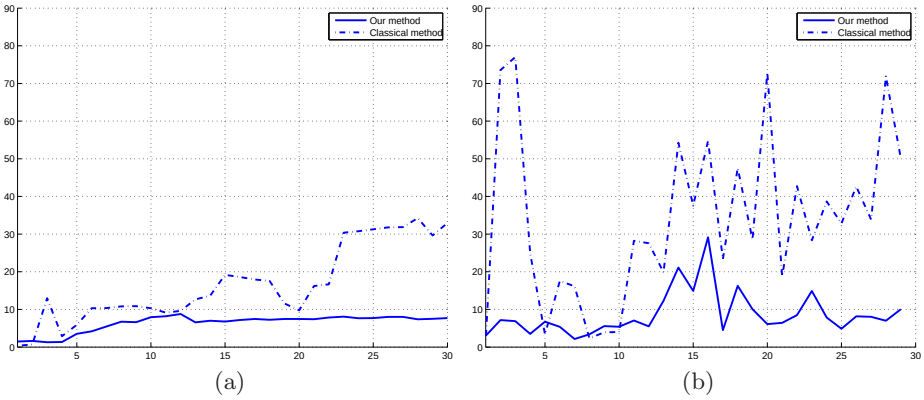

Fig. 11. Errors of the estimation: (a) rotation error and (b) translation error

3. Marchand, E., Chaumette, F.: Fitting 3d models on central catadioptric images. In: IEEE Int. Conf. on Robotics and Automation, ICRA'07, Rome, Italy (April 2007) 52–58
4. Nister, D., Naroditsky, O., Bergen, J.: Visual odometry. cvpr **01** (2004) 652–659
5. Lhuillier, M.: Automatic scene structure and camera motion using a catadioptric system. Comput. Vis. Image Underst. **109**(2) (2008) 186–203
6. Mei, C., Benhimane, S., Malis, E., Rives, P.: Constrained multiple planar template tracking for central catadioptric cameras. In: British Machine Vision Conference. (September 2006)
7. Daniilidis, K., Makadia, A., Bulow, T.: Image processing in catadioptric planes: Spatiotemporal derivatives and optical flow computation. In: Workshop on Omnidirectional Vision (in conjunction with ECCV 2002), Copenhagen (June 2002) 3–12
8. Bullow, T. In: Multiscale Image Processing on the Sphere. Volume 2449 of Lecture Notes in Computer Science. Springer Berlin - Heidelberg (2002) 609–617
9. Hansen, P.I., Corke, P., Boles, W., Daniilidis, K.: Scale invariant feature matching with wide angle images. In: IEEE/RSJ Int. Conf. on Intelligent Robots and Systems, IROS'07, San Diego, CA, USA (November 2007) 1689–1694
10. Klippenstein, J., Zhang, H.: Quantitative evaluation of feature extractors for visual slam. In: CRV '07: Proceedings of the Fourth Canadian Conference on Computer and Robot Vision, Washington, DC, USA, IEEE Computer Society (2007) 157–164
11. Mikolajczyk, K., Schmid, C.: A performance evaluation of local descriptors. IEEE Trans. Pattern Anal. Mach. Intell. **27**(10) (2005) 1615–1630
12. Geyer, C., Daniilidis, K.: A unifying theory for central panoramic systems and practical implications. In: European Conference on Computer Vision. Volume 29., Dublin, Ireland (May 2000) 159–179
13. Barreto, J., Araujo, H.: Geometric properties of central catadioptric line images. In: 7th European Conference on Computer Vision, ECCV'02, Copenhagen, Denmark (May 2002) 237–251
14. Chirikjian, G., Kyatkin, A.: Engineering Applications of Noncommutative Harmonic Analysis. CRC Press (2001)
15. Kostelec, P.J., Rockmore, D.N.: FFTs on the rotation group. Technical report, Santa Fe Institute (2003)
16. Wandelt, B.D., Gorski, K.M.: Fast convolution on the sphere. Physical Review D **63** (2001) 123002
17. Driscoll, J.R., Dennis M. Healy, J.: Computing fourier transforms and convolutions on the 2-sphere. Adv. Appl. Math. **15**(2) (1994) 202–250
18. Bülow, T.: Spherical diffusion for surface smoothing. In: First International Symposium on 3D data Processing, Visualizarion and Transmission
19. Koenderink, J.J., van Doom, A.J.: Representation of local geometry in the visual system. Biol. Cybern. **55**(6) (1987) 367–375
20. Schmid, C., Mohr, R., Bauckhage, C.: Evaluation of interest point detectors. International Journal of Computer Vision **37**(2) (2000) 151–172
21. Lowe, D.G.: Distinctive image features from scale-invariant keypoints. Int. J. Comput. Vision **60**(2) (2004) 91–110
22. Mei, C., Rives, P.: Single view point omnidirectional camera calibration from planar grids. In: IEEE International Conference on Robotics and Automation. (April 2007)
23. Stewénius, H., Engels, C., Nistér, D.: Recent developments on direct relative orientation. ISPRS Journal of Photogrammetry and Remote Sensing **60** (June 2006) 284–294